

Nanoscale

Accepted Manuscript



This is an *Accepted Manuscript*, which has been through the Royal Society of Chemistry peer review process and has been accepted for publication.

Accepted Manuscripts are published online shortly after acceptance, before technical editing, formatting and proof reading. Using this free service, authors can make their results available to the community, in citable form, before we publish the edited article. We will replace this *Accepted Manuscript* with the edited and formatted *Advance Article* as soon as it is available.

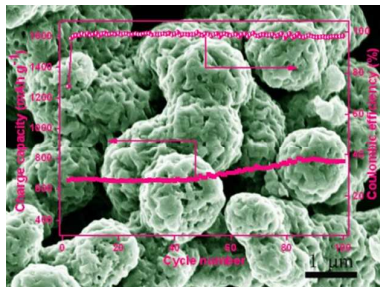
You can find more information about *Accepted Manuscripts* in the [Information for Authors](#).

Please note that technical editing may introduce minor changes to the text and/or graphics, which may alter content. The journal's standard [Terms & Conditions](#) and the [Ethical guidelines](#) still apply. In no event shall the Royal Society of Chemistry be held responsible for any errors or omissions in this *Accepted Manuscript* or any consequences arising from the use of any information it contains.

Graphical Abstract:

Direct large-scale synthesis of 3D hierarchical mesoporous NiO microspheres as high-performance anode materials for lithium ion batteries

Zhongchao bai,^{a*} Zhicheng Ju,^b Chunli Guo,^a Yitai Qian^c Bin Tang,^a Shenglin Xiong,^{c,d*}



3D hierarchical mesoporous NiO microspheres were scalable synthesized by thermal decomposition method; exhibit superior performance as anode material for LIBs.

Cite this: DOI: 10.1039/c0xx00000x

www.rsc.org/xxxxxx

ARTICLE TYPE

Direct large-scale synthesis of 3D hierarchical mesoporous NiO microspheres as high-performance anode materials for lithium ion batteriesZhongchao bai,^{a*} Zhicheng Ju,^b Chunli Guo,^a Yitai Qian,^c Bin Tang,^a Shenglin Xiong,^{c,d*}⁵ Received (in XXX, XXX) Xth XXXXXXXXX 20XX, Accepted Xth XXXXXXXXX 20XX

DOI: 10.1039/b000000x

Hierarchically porous materials have been an ideal material platform for constructing high performance Li-ion batteries (LIBs), offering great advantages of large contact area between the electrode and electrolyte, fast and flexible transport pathways for the electrolyte ions and the space for buffering the strain caused by repeated Li insertion/extraction. In this work, NiO microspheres with hierarchically porous structure have been synthesized via a facile thermal decomposition method only using a simple precursor. The superstructures are composed of nanocrystals with high specific surface area, pore volume, but broad pore size distribution. The electrochemical properties of 3D hierarchical mesoporous NiO microspheres were examined by cyclic voltammetry and galvanostatic charge-discharge studies. The results demonstrate that the as-prepared NiO nanospheres are excellent electrode materials in LIBs with high specific capacity, good retention and rate performance. The 3D hierarchical mesoporous NiO microspheres can still remain a reversible capacity of 800.2 mAh g⁻¹ after 100 cycles at a high current density of 500 mA g⁻¹.

Introduction

Hierarchically porous transition metal oxides have attracted great attention in the past few years because they are associated with improved efficiencies when used as catalysts, adsorbents or electrode materials in Li-ion batteries.¹⁻⁴ Especially, as electrode materials in LIBs, the porous materials have many unique advantages, including large contact area between electrode and electrolyte, fast and flexible transport pathways for the electrolyte ions and the space for buffering the strain caused by repeated Li insertion and extraction, because of their large surface area and porous profile.⁵⁻⁷ The general strategy to synthesize porous materials is hard/soft template-based or dealloying method.⁸⁻¹¹ All those methods are removing something from the host materials, and simultaneously generating the porous structures. However, those methods usually need strict experimental conditions or sophisticated post-treatment (such as removal of the template, selective etching in an appropriate solvent and cumbersome retreatment process), which not only introduce impurities and also increase the cost.¹²⁻¹⁵ More importantly, those methods are not suitable for large-scale production. Therefore, further research is still needed to develop novel strategy to fabricate porous materials. Recently, Thermal decomposition method (thermal decomposition of hydroxide, carbonate and oxalate etc.) is found to be an effective one to produce porous materials.¹⁶⁻¹⁹ Through this method, pores are generated accompanied by the release of gases (such as H₂O, CO₂ and CO etc.) during the thermal decomposition process. Compared with the template methods, this technique is simple, cost effective, and favorable for large-scale production. Thereby, such a strategy is more prospective than the template routes in industrial production. Nickel oxide (NiO) is considered to be a promising electrode material for lithium ion batteries and supercapacitors due to its low cost, low toxicity, and superior safety, in contrast to other transition metal oxides.²⁰⁻²⁵ Besides, the density of NiO is 6.67 g cm⁻³, leading to high volumetric energy density (approximately 5.8 times of graphite). Up to now, considerable efforts have been

done on the synthesis of nanostructure NiO and its composites for high performance LIBs.²⁶⁻²⁹ Wang et al. prepared NiO thin films made up of 30 nm nanoparticles using pulse laser ablation method and achieved a high discharge capacity of 700 mAh g⁻¹.²⁶ Yuan et al. fabricated spherical clusters of NiO nanoshafes through chemical precipitation followed by thermal decomposition, and discovered that the nanoshaf cluster electrodes had a higher reversible capacity than NiO nanopowders.²⁷ This result demonstrates that the structure and morphology have great effect on the electrochemical properties. Thus, more new strategies are needed to develop for devising NiO nanostructures to further improve their electrochemical performance. Most recently, several porous NiO nanostructures such as porous NiO nanowall films have been studied for lithium ion batteries by Huang et al.^{30,31} It is found that the porous NiO nanostructures show much better electrochemical performances than those dense counterparts owing to their large surface area and open edge geometry. And it is believed that the porous NiO nanostructures could exhibit superior lithium ion battery performance. However, all those methods need complicated procedures and substrates which cannot suit for scalable synthesis. Therefore, large-scale fabrication of porous NiO nanostructures via simple synthesis route is still a great challenge.

In this work, we report a facile and scalable method for the synthesis of 3D hierarchical porous NiO microspheres by thermal decomposition of Ni(CH₃COO)₂·4H₂O at 500 °C for 10 h. These mesoporous NiO spheres were characterized by XRD, TEM, SEM, and HRTEM to expound the detailed morphology and microstructure. Cyclic voltammograms (CVs), galvanostatic discharge/charge cycling and rate capability indicate that the porous NiO microspheres are excellent anode materials for high performance LIBs. The mesoporous NiO microspheres can still remain a reversible capacity of 800.2 mAh g⁻¹ after 100 cycles at a current density of 500 mA g⁻¹. To the best of our knowledge, this is the first report for the mass production of large-surface-area hierarchical architectures for NiO microspheres.

Experimental Section

Synthesis of 3D hierarchical porous NiO microspheres The reagent used in the experiments were analytical grade and used without further purification. The amount of precursor material $\text{Ni}(\text{CH}_3\text{COO})_2 \cdot 4\text{H}_2\text{O}$ was put into the crucible. The precursor was heated to 500 °C in air at a heating rate of 10 °C min^{-1} and then maintained at 500 °C for 10 h before being air-cooled to room temperature. Afterward, the gray green products were collected for structural characterization and the LIBs tests.

10 Electrochemical Investigation

The electrodes for electrochemical studies were prepared with 70 wt% active materials of the fabricated mesoporous NiO microspheres, 20 wt% conducting acetylene black, and 10 wt% carboxymethyl cellulose (CMC) binder in water. The slurry was pasted on a clean copper foil followed by drying in vacuum at 100 °C for 12 h. The coated foil was then roll-pressed and cut into a round slice. The cells were assembled using lithium foil as the counter electrode and the reference electrode, Celgard 2400 as the separator, and a solution of 1M LiPF₆ in a mixture of ethylene carbonate (EC)-ethyl methyl carbonate (EMC)-dimethyl carbonate (DMC) (1:1:1 by volume) as the electrolyte. The assembly of the cell was conducted in an argon-filled glove-box. The cells were charged and discharged from 0.01 to 3.0 V at different current densities (Land CT2001A). Cyclic voltammograms (CVs) were carried out on CHI-760 electrochemical workstation over the potential range 0.01–3.0 V at a scan rate of 0.1 mV s^{-1} .

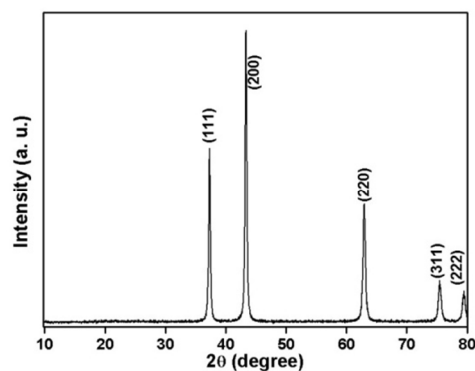
Structural Characterization

The samples were characterized by X-ray powder diffraction (XRD) with a Bruker D8 advanced X-ray diffractometer equipped with graphite-monochromatized Cu K α radiation ($K\alpha = 1.5418 \text{ \AA}$), recorded with the 2θ ranging from 10° to 80°. The scanning electron microscope images were taken with a JEOL JSM-7600F field-emission scanning electron microscope (FESEM). The high-resolution transmission electron microscope (HRTEM) images were recorded on a JEOL-2110 high-resolution transmission electron microscope at an acceleration voltage of 200 kV. The materials were further characterized by transmission electron microscopy (TEM) using JEOL-1011 microscope. Thermal gravimetric analysis (TGA) was carried out on a Mettler Toledo TGA/SDTA851 thermal analyzer apparatus and the heating rate is 10 °C min^{-1} . Nitrogen-sorption measurements were performed on a Tristar II 3020m gas sorptometer. Samples were degassed to 0.003 mmHg for 12 h at 608C. Specific surface areas were calculated by using the Brunauer–Emmett–Teller (BET) method, and pore sizes and volumes were estimated from pore-size distribution curves from the adsorption branches of the isotherms.

50 Results and discussion

XRD measurement was carried out to investigate the phase and structure of the prepared 3D hierarchical mesoporous NiO microspheres. Fig. 1 shows the XRD pattern of nickel acetate tetrahydrate after annealing at 500 °C in air for 10 h. All the diffraction peaks are in good agreement with the standard crystallographic data (JCPDS-No 04-0835, space group Fm3m), indicating nanocrystalline cubic structure of NiO. In addition, it

can be concluded that the nickel acetate tetrahydrate precursor has been fully transformed into crystalline NiO because no other diffraction peak is observed. This result is also confirmed by TGA examination. As shown in Figure 2, it can be observed that nickel acetate tetrahydrate precursor has decomposed completely at about 400 °C.



65 Fig. 1 the XRD pattern of the synthesized mesoporous NiO microspheres.

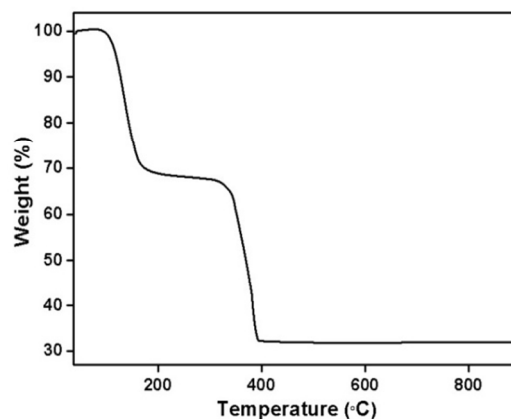


Fig. 2 TGA curves of the nickel acetate tetrahydrate under air.

The morphologies and nanostructures of the 3D hierarchical porous NiO microspheres were characterized by FESEM and TEM techniques. The low-magnification FESEM image (Fig. 3a) exhibits that the sample is composed of uniform microspheres with a diameter of 1-2 μm but coarse surfaces. The close observation (Fig. 3b) displays that the microspheres have a large number of holes in their bodies, producing 3D hierarchical porous spheres. A representative individual NiO sphere is shown in Fig. 3c, where the pores can be further determined by the distinct cavities, and the nanosized building blocks also can be clearly observed. Such an interesting porous structure is considered favorable in alleviating the large volume change originating from the conversion reaction during Li^+ insertion/extraction. Therefore, the electrochemical properties such as cycling performance and rate performance can be improved.^{32, 33} The porous structure of the NiO spheres is also revealed by the obvious contrast in the TEM image (Fig. 3d and e). A typical HRTEM image of porous NiO spheres is shown in Fig. 3f. The interplanar distance is 0.22 nm, which is in good agreement with (111) plane of cubic NiO.

Cite this: DOI: 10.1039/c0xx00000x

www.rsc.org/xxxxxx

ARTICLE TYPE

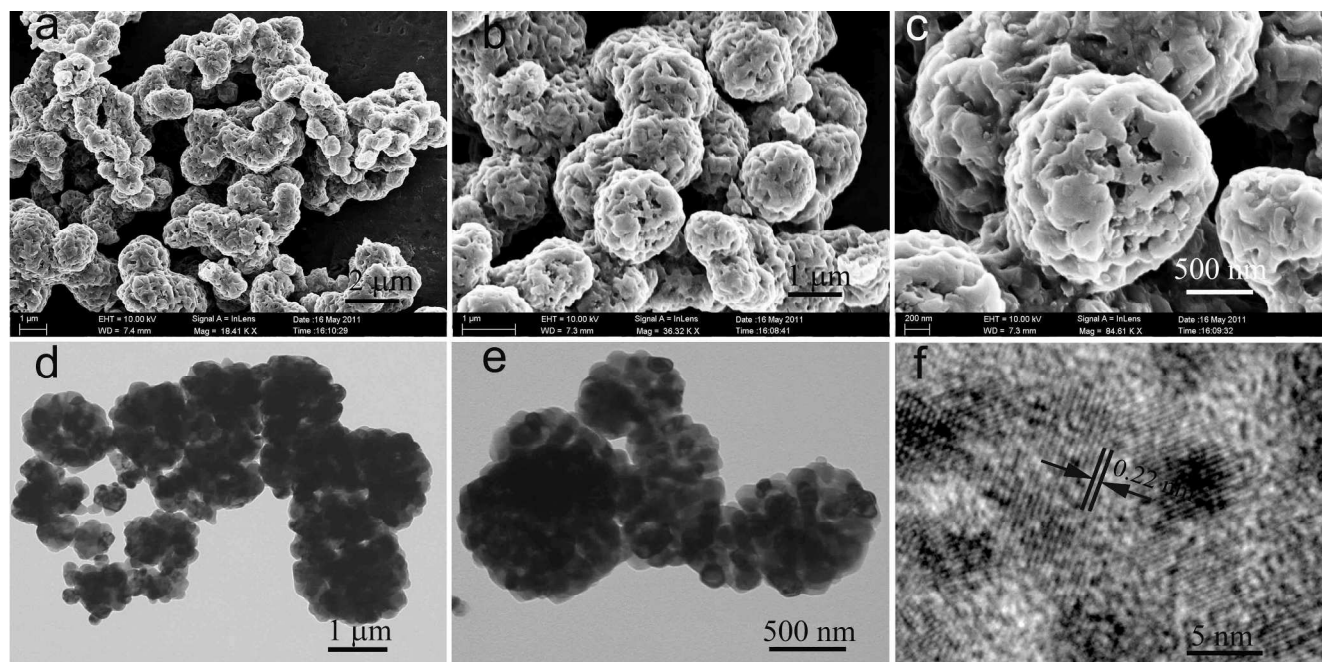


Fig. 3 (a) Low, (b) high-magnification, and (c) individual SEM images of the 3D hierarchical porous NiO microspheres; (d) low, (e) high-magnification TEM and (f) HRTEM images of the 3D hierarchical porous NiO microspheres.

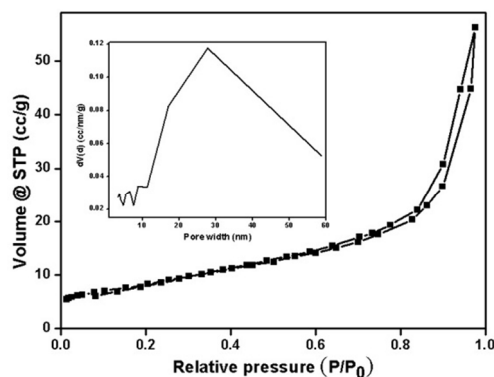


Fig. 4 N_2 adsorption isotherms and pore size distribution (insets) of mesoporous NiO microspheres

The mesoporous structure of the synthesized 3D hierarchical porous NiO microspheres was further studied by nitrogen adsorption-desorption measurements and shown in Fig. 4. NiO microspheres present isotherm of type IV with broad hysteresis loops (Fig. 4) which is associated with capillary condensation always happening in mesopore structures.^{34,35} The NiO sample displays a high surface area of $30.27 \text{ m}^2 \text{ g}^{-1}$ and total pore volume of $0.081 \text{ cm}^3 \text{ g}^{-1}$. The pore size distribution is inserted in Fig. 4 calculated from adsorption isotherms. Due to the high synthesis temperature of NiO spheres, the as-generated pores are less controlled, leading to a multi-modal pore size distribution. Because of the large surface area and porous structure, the as-synthesized 3D hierarchical NiO spheres may have many potential applications such as electrochemical supercapacitor and high performance LIBs, since they can offer unique advantages for the ion transfer at the electrode/electrolyte interface.

15

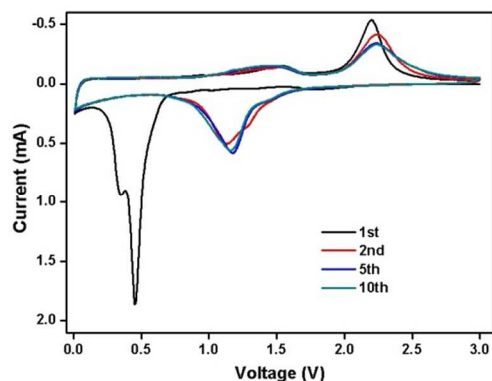
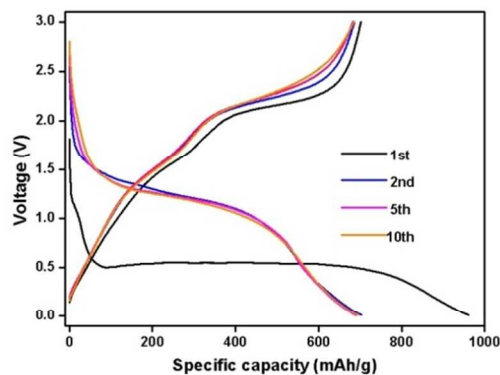


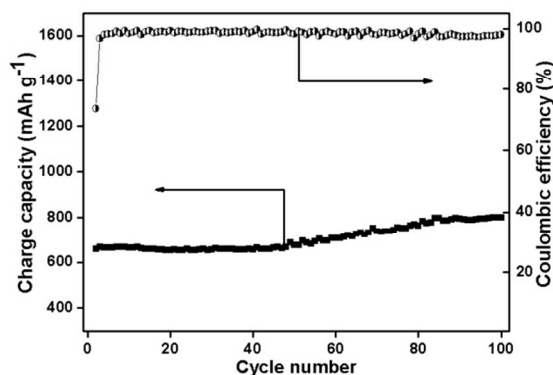
Fig. 5 Cyclic voltammograms of the mesoporous NiO spheres in the voltage range of 0.01-3.0V at a scan rate 0.1 mV s^{-1} .

The electrochemical properties of the obtained 3D hierarchical porous NiO microspheres were studied systematically. To understand its reaction mechanism during electrochemical charge/discharge process, CVs studies were conducted in half-cell configuration (Li/NiO) over a voltage range from 0.01 to 3.0 V vs. Li at a slow scan rate of 0.1 mV s^{-1} (Fig. 5). During first cathodic sweep, two peaks are observed at around 0.46 and 0.35 V, respectively. The strong peak at 0.46 V corresponds to the initial reduction of NiO to Ni accompanied with the formation of amorphous Li_2O , and electrolyte decomposition to form the solid electrolyte interphase (SEI) layer.^{28, 36} The relative weak peak at 0.35 V might be attributed to the structural destruction and disappears in the subsequent scans.³⁷ The discharge plateau shifted to 1.15 V during the following cycles which may be related to the drastic lithium-driven structural or textural modifications. For the anodic scans, the broad and weak peak located at 1.43 V should be ascribed to the dissolution of the organic SEI layer,³⁸ while the peak at 2.24 V is attributed to the oxidation of Ni^0 to Ni^{2+} along with the decomposition of Li_2O .²¹ Nevertheless, the oxidation peaks do not change much in the subsequent cycles compared with the first scan, suggesting the similar electrochemical reactions in the anodic scans. The CV curves are stable and well overlapped after the second cycle, indicating high electrochemical reversibility and good capacity retention for the mesoporous NiO electrodes.

a



b



15

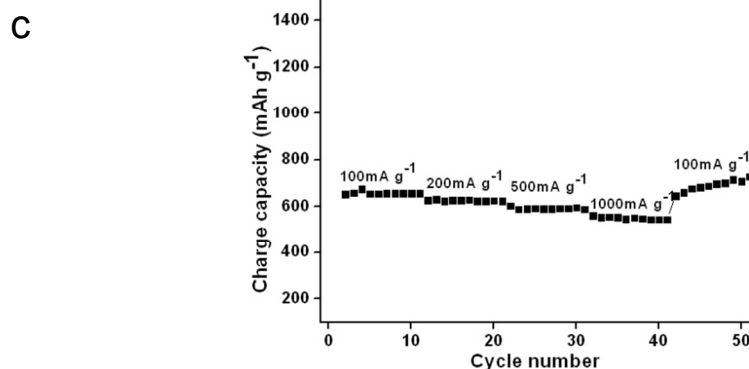


Fig. 6 (a) The 1st, 2nd, 5th and 10th voltage profiles of the mesoporous NiO electrode between 0.01 and 3 V at the current density of 500 mA g⁻¹. Galvanostatic discharge–charge cycling was carried out in the voltage range from 0.01 to 3.0 V. (b) Cycle performance and coulombic efficiency versus cycle number of mesoporous NiO electrode at a current density of 500 mA g⁻¹. (c) Rate capabilities with increasing current density of the porous NiO electrode.

Fig. 6a shows the discharge–charge voltage profiles of the 1st, 2nd and 10th cycles for the mesoporous NiO electrode, which cycled between 0.01 and 3 V at a current density of 500 mA g⁻¹. In the first discharge, the curve begins from the open circuit voltage and quickly decreases to the plateau about 0.5 V with a capacity of 102 mAh g⁻¹. This result may relate to forming the lithiated NiO. The main reaction of lithium and NiO occurs in the voltage plateau around 0.5 V corresponds to the reduction of Ni²⁺ to Ni⁰. A total capacity of 961.2 mAh g⁻¹ is delivered, which is higher than the theoretical capacity of 718 mAh g⁻¹. It is possible that the extra capacity was contributed by the formation of a polymer-like SEI layer.³⁹ The first charge curve from 0.01 to 3.00 V shows a steady and smooth voltage increase (overall capacity of 702 mAh g⁻¹). Therefore, there is a capacity loss of 30.9% in the first cycle, which can be mainly attributed to the possible irreversible processes such as electrolyte decomposition and inevitable formation of a SEI layer. In the second discharge cycle, the major potential plateau shifts to about 1.2 V (versus Li⁺/Li) because of the structural or textural rearrangement.⁴⁰ After the second cycle, the voltage profiles are almost the same compared with the second cycle. This result agrees well with the CV measurements.

Fig. 6b displays the cycling performance of the mesoporous NiO microspheres at the current density of 500 mA g⁻¹. The electrode shows a steady capacity about 660 mAh g⁻¹ at the initial 40 cycles. Afterwards, the charge capacity gradually increases until the 80th cycle. Hereafter, the electrode shows exceptional cycling performance with high coulombic efficiency (higher than 98%). The increasing specific capacity may be due to the reversible growth of a polymeric gel-like layer originating from kinetically activated electrolyte degradation and the interfacial lithium storage, which is common for most anode materials.^{41–43} Finally, the electrode maintains a specific capacity of 800.2 mAh g⁻¹ after 100 cycles, which is larger than the previously reported values for NiO nanomaterials, such as spray pyrolyzed NiO-C nanocomposite furnished with a capacity below 500 mAh g⁻¹ at the current density of 400 mA g⁻¹ after 50 cycles,⁴⁴ MgO coated NiO nanocrystalline thin film delivering a capacity of 750 mAh g⁻¹ after 150 cycles at 0.5 C,⁴⁵ Nanostructured NiO achieving reversible capacity of 783 mA h g⁻¹ after 50 cycles at the low rate of 0.2 C,⁴⁶ and the NiO-graphene hybrid electrode with a capacity of 646.1 mA h g⁻¹ after 35 cycles at a current density of 100 mA g⁻¹.⁴⁷ The enhanced performance of the mesoporous NiO spheres may come from its porous structure, which provides efficient electrolyte ions transport pathways, large surface-to-volume ratio, and effective tolerance to the volume change when lithium ions diffuse into/out the electrode.^{48,49} Most importantly, the structure of mesoporous NiO microspheres was roughly maintained after 50 cycles at 500 mA g⁻¹, as shown in Figure 7, illustrating its structural stability of the mesoporous spheres through long cycling process at high current density.

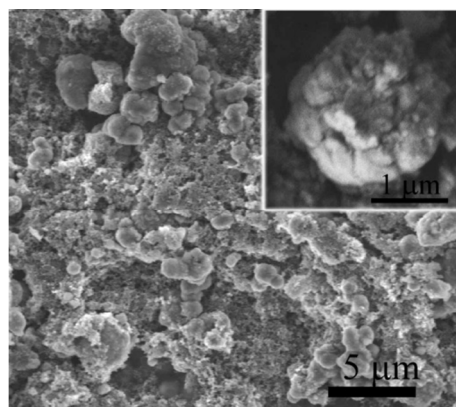


Fig. 7 SEM image of the electrodes after 50 cycles at a current density of 500 mA g⁻¹.

High rate performance is another important precondition to apply as anode material in high power Li-ion batteries. Therefore, the prepared 3D hierarchical porous NiO spheres were examined with different current densities in ambient temperature conditions, and the results were given in Fig. 6c. As expected, the synthesized porous NiO spheres show good rate performance. The capacity is stable during cycling irrespective of the current densities applied. The discharge capacities of mesoporous NiO microspheres at 100, 200, 500,

and 1000 mA g⁻¹ were 725, 694, 662, and 621 mAh g⁻¹, respectively, demonstrating an excellent high rate performance for high power lithium ion battery. It should be noticed that as long as the current rate reversed back to low current rate, the cell capacity recovered to the original values, indicating that the integrity of mesoporous NiO crystals has been preserved even after high rate cycling. This implies that mesoporous NiO crystals are tolerant of various charge and discharge currents, which is preferred for high power applications.

Conclusions

In summary, a cheap and scalable method for the fabrication of 3D hierarchical porous NiO spheres has been developed. The obtained 3D hierarchical porous NiO spheres maintain a high reversible capacity of 800.2 mAh g⁻¹ at the high current density of 500mA g⁻¹ after 100 cycles, and exhibit excellent cycling stability and good rate capability. The enhanced electrochemical performance can be ascribed to the unique 3D hierarchical porous structure, which offers the fast and flexible transport pathways for the electrolyte ions, and sufficient free space to accommodate the volume change upon lithium-ion insertion/extraction. The excellent cycling stability and good rate capability make such 3D hierarchical porous NiO spheres a promising anode material for next-generation lithium-ion batteries. This facile strategy may be extended to synthesize other transition metal oxides with porous architectures, which are very prospective in high performance rechargeable LIBs or catalyst because of their unique structural features.

Acknowledgments

This work was supported by the 973 Project of China (No. 2011CB935901), the National Nature Science Foundations of China (No. 91022033, 21201129, and 201371108), Science and Technology Committee of Shanxi Province (No.20110321051), Technology Development, China, Project (2011-038), Shandong Provincial Natural Science Foundation for Distinguished Young Scholar, the Independent Innovation Foundations of Shandong University (No.2012ZD008), the National Science Foundation of Shandong Province (No. ZR2012BM018), and the Opening Project of CAS Key Laboratory of Materials for Energy Conversion. Natural Science Youth Foundation of Shanxi Province (2013021011-4 and 2013011012-3)

Notes and references

- ^a Research Institute of Surface Engineering, Taiyuan University of Technology, Taiyuan, 030024, China. Tel.: +86 351 6010540. E-mail: baizhongchao@tyut.edu.cn
- ^b School of Materials Science and Engineering, China University of Mining and Technology, Xuzhou 221116, P. R. China.
- ^c Key Laboratory of the Colloid and Interface Chemistry (Shandong University), Ministry of Education, and School of Chemistry and Chemical Engineering, Shandong University, Jinan, 250100, PR China.
- ^d CAS Key Laboratory of Materials for Energy Conversion. Email: chexsl@sdu.edu.cn.
- E. S. Toberer, T. D. Schladt, and R. Seshadri, *J. Am. Chem. Soc.*, 2006, **128**, 1462.
- Y. Ren, Z. Ma, R. E. Morris, Z. Liu, F. Jiao, S. Dai and P. G. Bruce, *Nat. Commun.*, 2013, DOI: 10.1038/ncomms3015.
- Z. C. Bai, B. Sun, N. Fan, Z. C. Ju, M. H. Li, L. Q. Xu, and Y. T. Qian, *Chem. Eur. J.*, 2012, **18**, 5319.
- H. B. Wu, H. Pang and X. W. Lou, *Energy Environ. Sci.*, 2013, DOI: 10.1039/C3EE42101E.
- L. Hu, H. Zhong, X. R. Zheng, Y.M. Huang, P. Zhang and Q. W. Chen, *Sci Rep.*, 2013, doi:10.1038/srep00986.
- Y. G. Wang, H. Q. Li, P. He, E. Hosono and H. S. Zhou, *Nanoscale*, 2010, **2**, 1294.
- Z. C. Bai, N. Fan, Z. C. Ju, C. L. Guo, Y. T. Qian, B. Tang and S. L. Xiong, *J. Mater. Chem. A*, 2013, **1**, 10985.
- F. Jiao, J. C. Jumas, M. Womes, A. V. Chadwick, A. Harrison, and P. G. Bruce, *J. Am. Chem. Soc.*, 2006, **128**, 12905.
- C. L. Xu, Y. Q. Zhao, G. W. Yang, F. S. Li, and H. H. Li, *Chem. Commun.*, 2009, 7575.
- B. Z. Tian, X. Y. Liu, B. Tu, C. Z. Yu, J. Fan, L. M. Wang, S. H. Xie, G. D. Stucky, D. Y. Zhao, *Nat. Mater.* 2003, **2**, 159.
- J. T. Zhang, P.P. Liu, H.Y. Ma, and Y. Ding, *J. Phys. Chem. C*, 2007, **111**, 10382.
- C. C. Yu, X. P. Dong, L. L. Guo, J. T. Li, F. Qin, L. X. Zhang, J. L. Shi, and D. S. Yan, *J. Phys. Chem. C*, 2008, **112**, 13378.
- J. P. Xie, Q. B. Zhang, W. J. Zhou, J. Y. Lee, and D. I. C. T. Wang, *Langmuir*, 2009, **25**, 6454.
- S. Pruneanu, L. Olenic, S. A. F. Al-Said, G. Borodi, A. Houlton, and B. R. Horrocks, *J. Mater. Sci.*, 2010, **45**, 3151.
- B. Z. Tian, X. Y. Liu, L. A. Solovyov, Z. Liu, H. F. Yang, Z. D. Zhang, S. H. Xie, F. Q. Zhang, B. Tu, C. Z. Yu, O. Terasaki, and D. Y. Zhao, *J. Am. Chem. Soc.*, 2004, **126**, 865.
- C. C. Yu, L. X. Zhang, J. L. Shi, J. J. Zhao, J. H. Gao, and D. S. Yan, *Adv. Funct. Mater.*, 2008, **18**, 1544.
- L. P. Zhu, G. H. Liao, Y. Yang, H. M. Xiao, J. F. Wang, and S. Y. Fu, *Nanoscale Res. Lett.*, 2009, **4**, 550.
- Z. H. Yang, W. X. Zhang, Q. Wang, X. M. Song, and Y. T. Qian, *Chem. Phys. Lett.* 2006, **418**, 46.
- Q. R. Zhao, Z. G. Zhang, T. Dong, and Y. Xie, *J. Phys. Chem. B*, 2006, **110**, 15152.
- X. F. Li, A. Dhanabalan and C. L. Wang, *J. Power Sources* 2011, **196**, 9625.
- X. H. Wang, L. Qiao, X. L. Sun, X. W. Li, D. K. Hu, Q. Zhang and D. Y. He. *J. Mater. Chem. A*, 2013, **1**, 4173.
- D. W. Su, M. Ford, and G. X. Wang, *Sci. Rep.*, 2012, **2**, 924.
- H. B. Wu, J. S. Chen, H. H. Hng and X. W. Lou, *Nanoscale*, 2012, **4**, 2526.
- G. Q. Zhang, L. Yu, H. E. Hoster and X. W. Lou, *Nanoscale*, 2013, **5**, 877.
- B. Wang, J. S. Chen, Z. Y. Wang, S.n Madhavi, X. W. Lou, *Adv. Energy Mater.*, 2012, **2**, 1188.
- Y. Wang, and Q. Z. Qin, *J. Electrochem. Soc.*, 2002, **149**, A873.
- L. Yuan, Z. P. Guo, K. Konstantinov, P. Munroe, H. K. Liu, *Electrochem. Solid-State Lett.*, 2006, **9**, A524.
- X. H. Huang, J. P. Tu, B. Zhang, C. Q. Zhang, Y. Li, Y. F. Yuan, H. M. Wu, *J. Power Sources*, 2006, **161**, 541.
- X. H. Huang, J. P. Tu, C. Q. Zhang, J. Y. Xiang, *Electrochem. Commun.*, 2007, **9**, 1180.

30. P. R. Bueno and E. R. Leite, *J. Phys. Chem. B*, 2003, **107**, 8868.
31. P. Poizot, S. Laruelle, S. Grugeon, L. Dupont and J. M. Tarascon, *Nature*, 2000, **407**, 496.
32. X. W. Lou, L. A. Archer and Z. C. Yang, *Adv. Mater.*, 2008, **20**, 3987.
33. J. Liu, F. Liu, K. Gao, J. S. Wu and D. F. Xue, *J. Mater. Chem.*, 2009, **19**, 6073.
- 5 34. M. B. Zakaria, N. Suzuki, N. L. Torad, M. Matsuura, K. Maekawa, H. anabe, and Y. Yamauchi, *Eur. J. Inorg. Chem.*, 2013, 2330.
35. K. S. W. Sling, D. H. Everett, R. A. W. Haul, L. Moscou, R. A. Pierotti, J. Rouquerol, and T. Siemieniowska, *Pure & Appl. Chem.*, 1985, **57**, 603.
36. B. Varghese, M. V. Reddy, Z. Yanwu, C. S. Lit, T. C. Hoong, G. V. S. Rao, B. V. R. Chowdari, A. T. S. Wee, C. T. Lim and C. H. Sow, *Chem. Mater.*, 2008, **20**, 3360.
- 10 37. X. H. Huang, J. P. Tu, X. H. Xia, X. L. Wang, J. Y. Xiang, L. Zhang, Y. Zhou, *J. Power Sources*, 2009, **188**, 588.
38. X. Y. Yan, X. L. Tong, J. Wang, C. W. Gong, M. G. Zhang, L. P. Liang, *J. Alloys Compd.* 2013, **556**, 56.
39. Z. C. Bai, N. Fan, C. H. Sun, Z. C. Ju, C. L. Guo, J. Yang and Y. T. Qian, *Nanoscale*, 2013, **5**, 2442.
40. G. Binotto, D. Larcher, A. S. Prakash, R. Herrera Urbina, M. S. Hegde, and J. M. Tarascon, *Chem. Mater.*, 2007, **19**, 3032.
- 15 41. L. Li, K. H. Seng, Z. X. Chen, Z. P. Guo and H. K. Liu, *Nanoscale*, 2013, **5**, 1922.
42. L. Hu, H. Zhong, X. R. Zheng, Y. Huang, P. Zhang and Q. W. Chen, *Sci. Rep.*, 2013, DOI: 10.1038/srep00986
43. W. Wei , S. B. Yang , H. X. Zhou , I. Lieberwirth , X. L. Feng and K. Müllen, *Adv. Mater.*, 2013, DOI: 10.1002/adma.201300445
44. M. M. Rahman, S. L. Chou, C. Zhong, J. Z. Wang, D. Wexler, H. K. Liu, *Solid State Ionics*, 2010, **180**, 1646.
45. Y. Wang, Y. F. Zhang, H. R. Liu, S. J. Yu, and Q. Z. Qin, *Electrochim Acta*, 2003, **48**, 4253.
- 20 46. X. H. Wang, X. W. Li, X. L. Sun, F. Li, Q. M. Liu, Q. Wang and D. Y. He, *J. Mater. Chem.*, 2011, **21**, 3571.
47. Y. J. Mai, S. J. Shi, D. Zhang, Y. Lu, C. D. Gu, and J. P. Tu, *J. Power Sources*, 2012, **204**, 155.
48. D. Q. Zhang, M. C. Wen, P. Zhang, J. Zhu, G. S. Li, and H. X. Li. *Langmuir*, 2012, **28**, 4543.
49. J. S. Chen, H. Liu, S. Z. Qiao, and Lou, X. W. *J. Mater. Chem.*, 2011, **21**, 5687.

25

30

35

40

45